ELSEVIER

Contents lists available at ScienceDirect

Biosensors and Bioelectronics

journal homepage: www.elsevier.com/locate/bios





Impedance sensing of antibiotic interactions with a pathogenic *E. coli* outer membrane supported bilayer

Surajit Ghosh ^{a,1}, Zeinab Mohamed ^{b,1}, Jung-Ho Shin ^c, Samavi Farnush Bint E Naser ^a, Karan Bali ^d, Tobias Dörr ^c, Róisín M. Owens ^d, Alberto Salleo ^e, Susan Daniel ^{a,b,*}

- ^a Robert F. Smith School of Chemical and Biomolecular Engineering, Cornell University, Ithaca, NY, USA
- b Meinig School of Biomedical Engineering, Cornell University, Ithaca, NY, USA
- ^c Weill Institute for Cell and Molecular Biology and Department of Microbiology, Cornell, University, Ithaca, NY, USA
- ^d Department of Chemical Engineering and Biotechnology, University of Cambridge, Cambridge, UK
- ^e Department of Materials Science and Engineering, Stanford University, Stanford, CA, USA

ARTICLE INFO

Keywords: Outer membrane vesicles Supported lipid bilayer Impedance spectroscopy PEDOT:PSS Antibiotic-membrane interactions

ABSTRACT

Antibiotic resistance is a growing global health concern due to the decreasing number of antibiotics available for therapeutic use as more drug-resistant bacteria develop. Changes in the membrane properties of Gram-negative bacteria can influence their response to antibiotics and give rise to resistance. Thus, understanding the interactions between the bacterial membrane and antibiotics is important for elucidating microbial membrane properties to use for designing novel antimicrobial drugs. To study bacterial membrane-antibiotic interactions, we created a surface-supported planar bacterial outer membrane model on an optically-transparent, conducting polymer surface (poly (3,4-ethylenedioxythiophene) polystyrene sulfonate (PEDOT:PSS)). This model enables membrane characterization using fluorescence microscopy and electrochemical impedance spectroscopy (EIS). The membrane platform is fabricated using outer membrane vesicles (OMVs) isolated from clinically relevant Gram-negative bacteria, enterohemorrhagic *Escherichia coli*. This approach enables us to mimic the native components of the bacterial membrane by incorporating native lipids, membrane proteins, and lipopolysaccharides. Using EIS, we determined membrane impedance and captured membrane-antibiotic interactions using the antibiotics polymyxin B, bacitracin, and meropenem. This sensor platform incorporates aspects of the biological complexity found in bacterial outer membranes and, by doing so, offers a powerful, biomimetic approach to the study of antimicrobial drug interactions.

1. Introduction

Gram-negative bacteria contain two membranes: an outer membrane (OM) and a cytoplasmic-facing inner membrane (IM). These membranes serve as important barriers to protect bacteria from their environment and mediate the selective transport of materials into and out of cells. The OM is an asymmetric bilayer, with the outer leaflet mainly comprised of lipopolysaccharides (LPS) and the inner leaflet containing phospholipids such as phosphatidylethanolamine, phosphatidylglycerol, and cardiolipin (Hiroshi Nikaido, 1985). Unlike Gram-positive bacteria, which only have a cytoplasmic membrane, the presence of the OM provides Gram-negative bacteria with an intrinsic resistance to many detergents and high-molecular weight antibiotics. As a result, there are fewer

anti-Gram-negative antibiotics in comparison to anti-Gram-positive compounds (Epand et al., 2016; Silhavy et al., 2010; Ishan Ghai, 2018). The emergence of multi-drug resistant bacteria further exacerbates the need for new antibiotics. Changes in the OM specifically, such as changes in OM gene expression (i.e. upregulation of porins) or changes in LPS chemical properties (i.e. charge modification), can greatly impact antibiotic efficacy (Delcour, 2009). The increasing prevalence of antibiotic resistance coupled with the significant role of the OM in modulating antibiotic treatment outcomes has resulted in renewed interests in understanding the membrane permeability rules that govern antibiotic efficacy. Such knowledge will be needed to develop antimicrobial compounds that effectively target the membrane (Hurdle et al., 2011).

^{*} Corresponding author. Robert F. Smith School of Chemical and Biomolecular Engineering, Cornell University, Ithaca, NY, USA. *E-mail address*: sd386@cornell.edu (S. Daniel).

 $^{^{1}}$ Contributed equally to this work.

To elucidate OM properties and antibiotic-membrane interactions, model membranes such as supported lipid bilayers (SLBs) are often used to simulate native membranes to study their intrinsic properties in a controlled fashion (Su et al., 2019; Hollmann et al., 2018; Castellana and Cremer, 2006; Ye et al., 2009). One main advantage of using the SLB platform is its two-dimensional planar geometry, which is compatible with quantitative surface techniques such as fluorescence microscopy (TIRFM) (Su et al., 2019; Orosz et al., 2016) and quartz crystal microbalance with dissipation (QCM-D) (Cho et al., 2010; Reimhult et al., 2006).

Recently, SLBs have also been coupled with impedance spectroscopy to measure electrical processes occurring across the membrane (i.e. ion transport and membrane disruption) that cannot be captured on traditional SLB surfaces, which are typically silica or mica (Gritsch et al., 1998; Puiggali-Jou et al., 2018; Lin et al., 2010, 2012; Terrettaz et al., 2003). SLB formation on conductive surfaces is often combined with the addition of a conducting polymer such as poly (3,4-ethylenedioxythiophene) polystyrene sulfonate (PEDOT:PSS). This polymer acts as a cushion for the SLB and serves as a transducer of ion-to-electron flow with low impedance, enabling label-free, electrical readouts of the system (Su et al., 2019; Pappa et al., 1021; Liu et al., 2020). PEDOT:PSS coupled with silica-coated surfaces have been used to monitor interactions between simple reconstituted bacterial model membranes and antibiotics in previous work (Su et al., 2019). However, to date no Gram-negative membrane models that capture the membrane complexities of the OM, especially those that arise in pathogenic strains, have been described.

We have developed an SLB platform that integrates the bacterial OM and PEDOT:PSS to enable the direct electrical readout of bilayer formation and antibiotic-OM interactions. Our approach uses outer membrane vesicles (OMVs) to study the OM because these vesicles retain many of the key characteristics of the OM, including its membrane asymmetry and the heterogeneous mixture of membrane-embedded proteins, non-truncated smooth-LPS, and native phospholipids. OMVs are naturally secreted from the OM of many Gram-negative bacteria and are essential for mediating microbial immune responses, virulence, transport processes, and antibiotic resistence (Jan 2017; Toyofuku et al., 1038). The use of OMVs for SLB formation on silica surfaces was previously established by our lab using both non-pathogenic and pathogenic Gram-negative bacteria (Hsia et al., 2016; Mohamed et al., 2021). Here, we expand on our previous efforts to demonstrate an OM SLB platform that is compatible with conductive surfaces while maintaining the compositional complexity of the OM and fluidity of lipid molecules within the membrane bilayer. Using this platform, we then replicate known antibiotic-membrane interactions using EIS. Our OM SLB platform uses OMVs isolated from enterohemorrhagic E. coli O157:H7 (EHEC), a strain that is responsible for the majority of E. coli-related outbreaks. SLBs formed from this strain were used to interrogate membrane-antibiotic interactions using three different antibiotics: polymyxin B (PMB), bacitracin (BAC), and meropenem (MER). This label-free approach provides a convenient platform to study microbial membrane properties and the interaction of antibiotics with clinically relevant bacterial outer membranes..

2. Materials and methods

2.1. Materials

Poly (3,4-ethylenedioxythiophene) polystyrene sulfonate, PEDOT: PSS (Clevios PH 1000), was obtained from Heraeus Clevios. 4-Dodecylbenzenesulfonic acid (DBSA), (3-Glycidyloxypropyl) trimethoxysilane (GOPS), ethylene glycol (EG), and Polyallylamine hydrochloride (PAH) were purchased from Sigma-Aldrich. POPG (1-palmitoyl-2-oleoyl-sn-glycero-3-phospho-(1'-rac-glycerol)), and DSPE-PEG5000 (1,2-dioleoyl-sn-glycero-3-phosphoethanolamine-N-[methoxy (polyethylene glycol)-5000] were purchased from Avanti Polar Lipids. Chloroform, sodium

chloride, and magnesium chloride were purchased from VWR. Polymyxin B and meropenem were purchased from Sigma-Aldrich and bacitracin was purchased from Merck. All chemicals were used without further purification. Patterned ITO electrodes on glass substrates were purchased from Xin Yan Technology Limited. Phosphate-buffered saline (PBS) with 2 mM MgCl₂ was used for all experiments unless otherwise noted.

2.2. Preparation of PEDOT:PSS suspension

A 95% v/v PEDOT:PSS, 5% v/v EG, 1% v/v GOPS and 0.002% v/v DBSA were mixed in a cleaned glass vial. The solution mixture was then placed in a bath sonicator (ultrasonic cleaner, VWR) for \sim 0.5 h and passed through a 0.45 μ m syringe filter (Thomas Scientific) before use.

2.3. PEDOT:PSS surface coating

To deposit PEDOT:PSS films on glass or patterned ITO electrode surfaces, cleaned glass slides/patterned ITO electrodes were treated with oxygen plasma (Harrick Plasma) under a maximum power of 29.6 W at $\sim\!700~\mu m$ for 2 min and then coated with PEDOT: PSS suspension by drop-cast at 2500 rpm for 30 s using a Spin-Coater (Apogee Spin coater). The PEDOT:PSS coated slides/electrodes were then baked at 140° for 1 h and then immersed in DI water for $\sim\!4$ h. Just before use, these slides/electrodes were dried with nitrogen stream and activated with oxygen plasma at 29.6 W, $\sim\!700~\mu m$ for 2 min. Finally, a PDMS well with an average area of $\sim\!0.785~cm^2$ was placed on the top of slides/electrodes and used to contain the buffer solutions as SLB formation proceeded.

2.4. Isolation and characterizations of outer membrane vesicles (OMVs)

Enterohemorrhagic *E. coli* strain O157:H7, which contains a mutation that prevents the production of the Shiga toxin, was obtained from The Dörr lab at Cornell University. OMV isolation was adapted from previously established in-house protocols (Mohamed et al., 2021). Briefly, *E. coli* bacteria were grown to late log phase in Luria-Bertani (LB) medium at 37 °C from overnight liquid cultures. Bacteria were pelleted by centrifugation at 5000 RPM/3360×g for 15 min using a Thermo Fisher Sorvall ST 8 R centrifuge and the supernatant was filtered using a 0.2 μ m polyethersulfone (PES) membrane filter. OMVs were isolated from the supernatant by ultracentrifugation for 3 h at 140,000×g in a Beckman Coulter Ultracentrifuge with a SW28 Ti Swinging Rotor at 4 °C. Pelleted OMVs were resuspended in 100 μ L PBS supplemented with MgCl₂. The suspension was again centrifuged for 30 min at 16,000×g at 4 °C to remove any remaining flagella and impurities. The supernatant containing the vesicles was collected and stored at -80 °C until use.

2.5. Formation of the bacterial outer membrane bilayer

Plasma-cleaned PEDOT:PSS coated glass slides or ITO electrodes were used as the substrates for supported lipid bilayer formation. First, PDMS (polydimethylsiloxane, 10:1 elastomer:cross-linker mixture of Sylgard 184) wells were attached to the cleaned slide. To deposit a positively charged PAH interlayer, plasma cleaned PEDOT:PSS coated slides or electrodes were incubated with $80-100~\mu L$ of PAH solution in 0.5 M NaCl (conc. 1–2 mg/mL) for 15 min at room temperature, followed by a washing step with DI water and finally with PBS buffer. To form the OMV bilayer, 80 µL of a solution containing 10⁸ OMV particles/ mL were added to the PAH layer in the well and incubated for 15 min. The PDMS wells were gently washed with PBS to remove excess unabsorbed OMV and then absorbed OMVs were ruptured by adding POPG-PEG5k liposomes at a concentration of 1 mg/mL to the well. This mixture was incubated for 1 h to ensure complete rupture and bilayer formation and finally rinsed with PBS containing 2 mM MgCl₂ to remove excess liposomes.

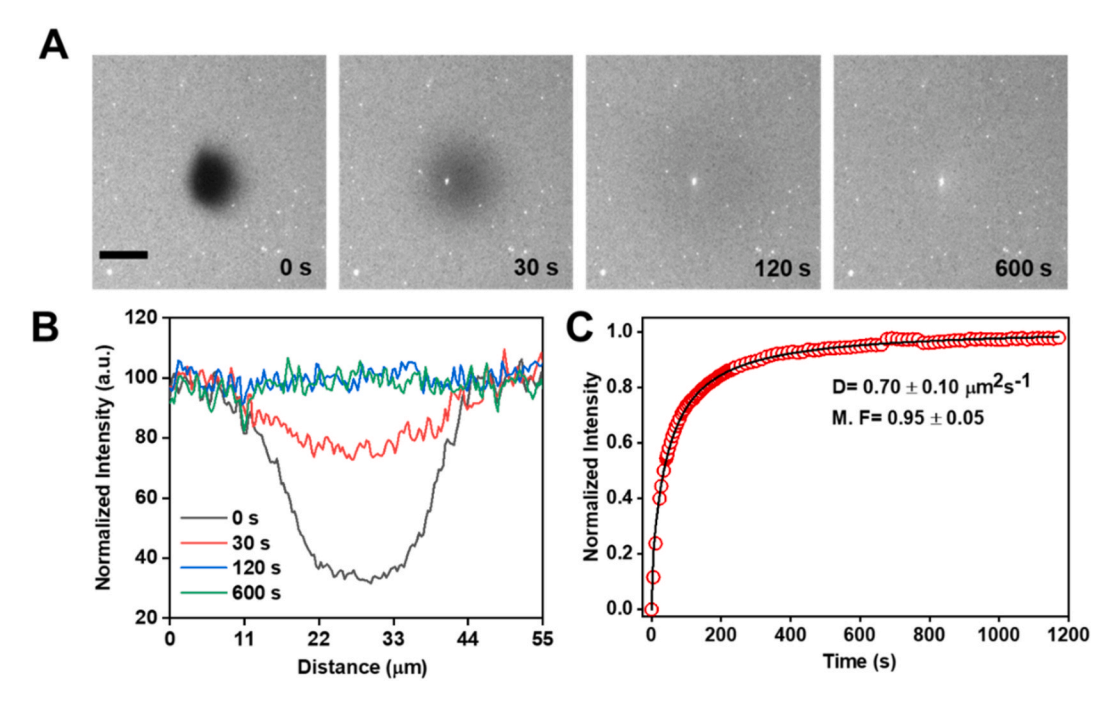


Fig. 1. Fluidity of OM bilayer on PAH/PEDOT:PSS. A) Images of fluorescence recovery of OM bilayer after photobleaching. Scale bar represents 20 µm. B) Line scans across the photobleached spot. C) Recovery curve of the fluorescence intensity over time fitted to a Soumpasis model (D = diffusion coefficient and M.F. = mobile fraction). Images and analysis of FRAP experiments for the control bilayer, POPG-PEG5K, can be found in the Supplemental Figures.

2.6. Fluorescence microscopy and FRAP for bilayer characterization

To confirm the formation of SLBs using OMVs on PEDOT:PSS surfaces, we utilized fluorescence microscopy and performed fluorescence recovery after photobleaching (FRAP) experiments. To visualize OMV rupture and subsequent SLB formation, we used the fluorescent marker octadecyl rhodamine B chloride (R18) to label the OMVs prior to rupture. The rupture process over time is observed as a transition from punctate fluorescent spots to a uniform fluorescence as the SLB is formed. After the formation of the SLB, the fluidity of the formed bilayers is measured by monitoring the recovery of a photobleached area of the bilayer over time. The FRAP instrument consists of an inverted Zeiss Axio Observer Z1 microscope with an α Plan-Apochromat 20 \times objective and 150 mW 561 nm optically pumped semiconductor laser (Coherent, Inc). Once the bilayer formed, the laser was used to photobleach a \sim 20 µm diameter spot at the z-plane and the fluorescence recovery of the photobleached area was recorded over time. Fluorescence intensity recovery data were then fit to the 2-D diffusion equation using the method of Soumpasis et al. (Soumpasis, 1983) The following equation was used to calculate the diffusion coefficient (D):

$$D = \frac{w^2}{t_{1_2}} \tag{1}$$

where w and $t_{\frac{1}{2}}$ represent the radius of the photobleached spot and the time required to achieve half of the maximum recovery intensity, respectively.

2.7. Antibody binding experiments

To confirm that the OM SLBs retained specific components of the outer membrane, fluorescent antibodies against lipid A and the outer membrane protein OMP were utilized in binding experiments while imaging with total internal reflection fluorescence microscopy (TIRFM). E. coli-derived OM supported bilayers formed on PAH coated PEDOT: PSS slides were first blocked with 2% bovine serum albumin for ~ 1 h to prevent non-specific antibody binding to the bilayer. The supported lipid bilayers were then rinsed with buffer (>5 mL) and primary

antibodies targeting outer membrane components (LPS and OMPs) were added and incubated for ~ 1 h. Unbound antibodies were rinsed away with buffer and fluorescent secondary antibodies (Abcam) were added to the bilayers for 1 h, then rinsed afterwards. Antibody binding was visualized on the surface of the bacterial bilayer using TIRFM and quantified using ImageJ (Schneider et al., 2012). Similar experiments were also carried out on POPG-PEG5K bilayer as a negative control under the same experimental conditions.

2.8. EIS measurements

Impedance spectra were recorded using a potentiostat (Autolab PGSTAT128N) equipped with a frequency response analysis module. Commercially available Ag/AgCl electrodes and a platinum mesh were used as the reference and counter electrode, respectively. PEDOT:PSS coated ITO served as the working electrode with an average area of $\sim\!0.785~{\rm cm}^2$. Electrochemical impedance spectra were recorded in the frequency range 10^5 to 0.1 Hz by superimposing an AC sinusoidal voltage of 10 mV. This frequency range was selected to capture frequency-dependent impedance changes of the OM bilayer ($\sim\!10^{-10}$ (Ishan Ghai, 2018) Hz), the electrode ($\sim\!<10~{\rm Hz}$) and the buffer ($\sim\!>10^4~{\rm Hz}$) to encompass the entirety of the system.

EIS was used to monitor every stage of bacterial outer membrane bilayer assembly on the PEDOT:PSS coated ITO electrode and to monitor the interaction of antibiotics with the formed bilayer. Stock solutions of PMB, BAC and MER were prepared at a concentration of 1 mg/mL in PBS. After formation of the bacterial model OM, the requisite amount of PMB or BAC was added to the well containing the bilayer to make the final concentration of antibiotics approximately 30 $\mu g/mL$. The bilayers were incubated with the antibiotics for 15 min at room temperature. For MER experiments, non-specific membrane interactions of MER were reduced by blocking the bilayers with 2% BSA for 1 h before incubating with MER for 1 h at a concentration of 100 $\mu g/mL$. Finally, excess/unbound antibody was rinsed with buffer and impedance measurements were taken again. The measured impedance spectra were fitted to an equivalent circuit model using the Metrohm Autolab NOVA (v 2.1.4) software.

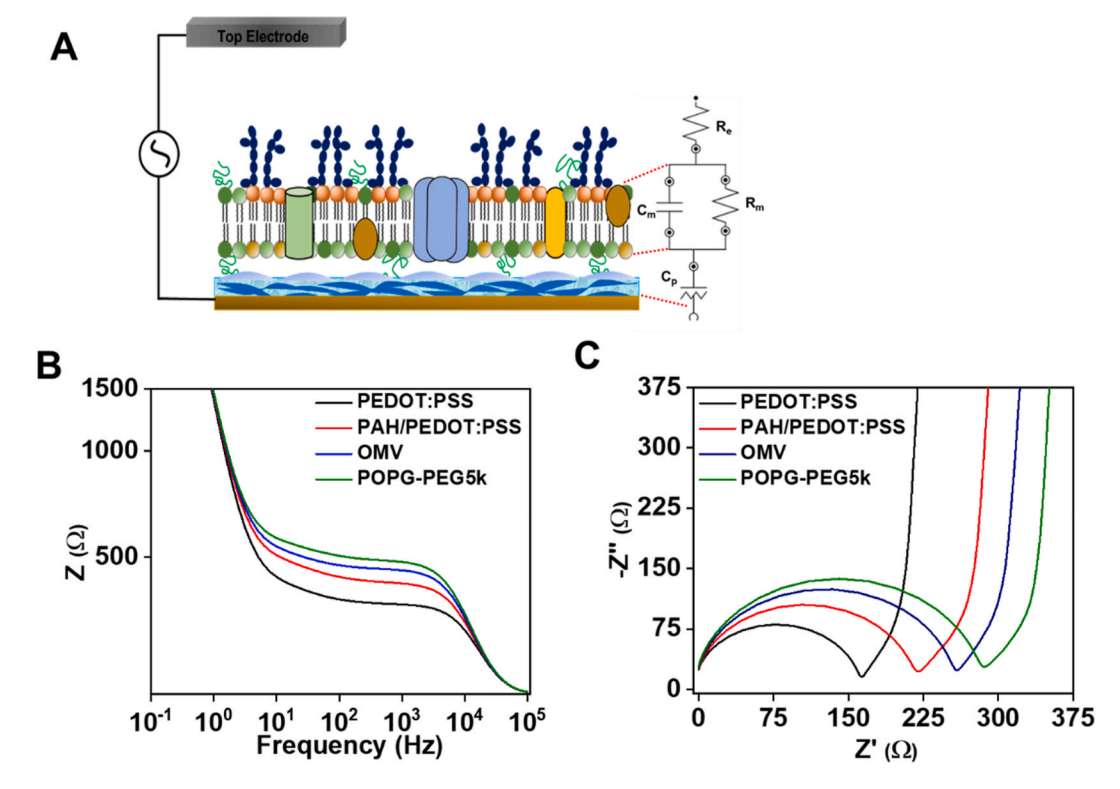


Fig. 2. EIS monitoring of OM-bilayer formation on PEDOT:PSS coated ITO electrode. (A) Schematic of OM-bilayer formation on PEDOT:PSS coated ITO and its representation as an equivalent circuit. (B) Bode and (C) Nyquist plots showing the impedance at each stage of bacterial OM bilayer formation.

3. Results and discussion

3.1. Fluid bacterial OM bilayers can be formed on conducting polymer surfaces

OMVs released from bacterial outer membranes retain their native membrane properties; they contain LPS, various outer membrane proteins, and the same composition of phospholipids (Fig. S1) (McBroom et al., 2006; Nagakubo et al., 2019; SchwechheimerKuehn, 2017) Due to their proteinaceous lipid membranes and negative surface charge, OMVs are unable to rupture spontaneously to form planar OM bilayers on glass or PEDOT:PSS surfaces, as these both bear a negative charge. However, fusogenic zwitterionic liposomes can induce bilayer formation from proteoliposomes and mammalian cell-derived blebs on silica and PEDOT:PSS coated surfaces via vesicle fusion (Su et al., 2019; Pappa et al., 1021; Hsia et al., 2016; Liu et al., 2017; Uribe et al., 2020). We adapted this approach to form OM bilayers on PEDOT:PSS using OMVs that ruptured in the presence of fusogenic liposomes. Liposomes consisting primarily of phosphatidylglycerol (POPG) were chosen to mimic the lipids of the native bacterial OM. These liposomes were additionally doped with 0.5 mol% of DSPE-PEG5000, an inert polyethylene glycol group attached to the lipid head group, to serve as a cushion between the surface and the planar lipid bilayer and foster two-dimensional fluidity in the bilayer. To promote spontaneous rupture and fusion of POPG-PEG5K liposomes, we introduced a cationic polyelectrolyte interlayer between the surface and the liposomes to reduce electrostatic repulsion to the PEDOT:PSS surface (Fig. S3). Cationic polyelectrolytes are popular as coating materials for surface modification, adhere onto negatively charged surfaces, and are compatible with supported lipid bilayer formation (Diamanti et al., 2016; Pappa et al., 2017; Heath et al., 2016; Zhang et al., 2000, 2002). Here, we use the polyelectrolyte polyallylamine hydrochloride (PAH) to coat the negatively-charged PEDOT:PSS surface. The PAH coating promotes spontaneous rupture of POPG-PEG5K liposomes following OMV adsorption, resulting in the formation of a planar bacterial membrane model that contains the lipids,

proteins, and lipopolysaccharides from the bacterial OM (Fig. S2).

As a confirmation of liposome and OMV rupture, and determination of membrane fluidity, we performed fluorescence recovery after photobleaching (FRAP) experiments on the fluorescently labeled OM bilayer and characterized its two-dimensional diffusion coefficient (Fig. 1A and Fig. 1B). The diffusion coefficient of the OM bilayer was found to be 0.70 \pm 0.10 $\mu m2/s$ with a mobile fraction of 95 \pm 5% (Fig. 1C). In comparison, the POPG-PEG5K control bilayer (in the absence of OMVs) on PAH/PEDOT:PSS yielded an average diffusion coefficient of 0.92 \pm 0.09 $\mu m^2/s$ with a mobile fraction of 97 \pm 5% (Fig. S4). Mobile fractions were high in both cases, indicating that the bilayers are relatively free of unruptured vesicles. The diffusion coefficient for the OM bilayer on PAH/PEDOT:PSS was slightly less than the liposome bilayer (control) likely due to the presence of OM components in the former.

3.2. The formation of the OM bilayer can be monitored using EIS

In addition to fluorescence confirmation of OM bilayer formation, we used EIS to track the formation of OM bilayers on PAH/PEDOT:PSS-coated ITO electrodes (Fig. 2A). Impedance associated with each step of OM bilayer formation can be measured and used to monitor bilayer formation, as shifts to higher impedances indicate the presence of insulating materials on the electrode surface that impact ion transfer to the electrode. We collected impedance data for PEDOT:PSS in the desired buffer solution (PBS + 0.2 mM MgCl₂) as the baseline and then again for PEDOT:PSS with PAH coating. The addition of the PAH layer on top of PEDOT:PSS resulted in a small shift towards higher impedance due to the presence of the layer reducing ion flow directly to the electrode. The adsorption of OMVs on PAH further increased impedance. With the addition of fusogenic POPG-PEG5K liposomes, the rupture of OMVs leads to higher impedance as the formation of the bilayer on the electrode surface reduces ionic flux to the conducting polymer.

Bode and Nyquist plots for each step in the bilayer formation process are shown in Fig. 2B and C. Nyquist plots show the negative of the imaginary impedance plotted against real impedance for each frequency

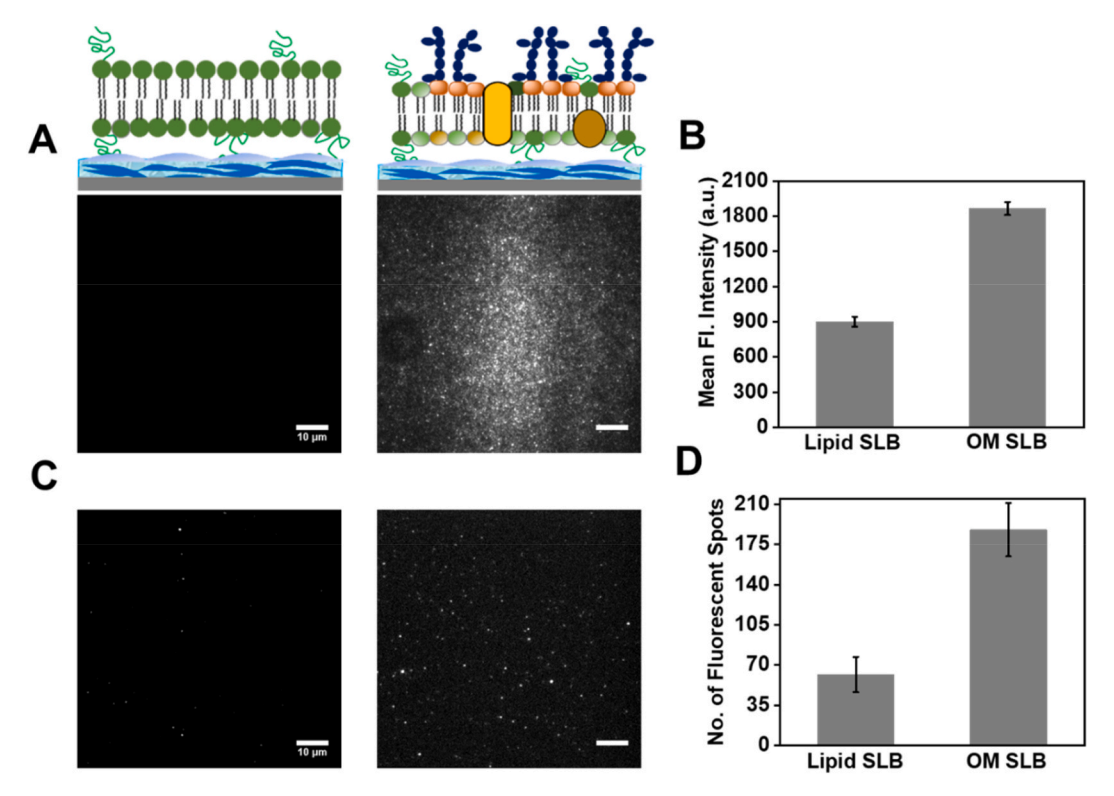


Fig. 3. Retention of LPS and outer membrane proteins in OM bilayer formed on PAH/PEDOT:PSS A) TIRFM images of control (left) and bacterial OM (right) lipid bilayers following incubation with anti-lipid A antibody. B) Quantified fluorescence signal from in TIRFM images. C) TIRFM images of control (left) and bacterial OM (right) lipid bilayers following incubation with anti-OMP. D) Quantified number of fluorescent particles from TIRM images analyzed via ImageJ. Error bars represent standard deviation. Scale bars represent 20 µm.

measurement. Bode plots provide the frequency response of the magnitude of impedance (or phase). These plots can be used to extract the electrical properties of the membrane using an equivalent circuit model for the system (See Supporting Information for details and Fig. S11). We note that membranes are typically modeled as a resistor (R_m) in parallel with a capacitor (C_m) (Pappa et al., 1021; Liu et al., 2020; Zhang et al., 2016). The calculated resistance and capacitance values of the OM bilayers on these devices are 230 Ω cm² and 70 nF cm⁻², respectively. For comparison, we also calculated the resistance and capacitance values of the POPG-PEG5K control bilayer, which are 323.42 Ω cm² and 78 nF cm⁻², respectively (Fig. S5). The resistance of the control POPG-PEG5K bilayer was higher than that of the bacterial OM bilayer. This may be due to the higher permeability of the OM compared to pure lipid bilayers and the presence of native membrane components, such as porins, that facilitate ion transport through the OM (Silhavy et al., 2010). The resistance calculated for the POPG-PEG5K bilayer is comparable to published values reported using POPG-POPE bilayers on PEDOT:PSS (Su et al., 2019). Additionally, the capacitance of the OM bilayer was slightly lower than the capacitance of the POPG-PEG5K bilayer, which is likely due to the OM bilayer being thicker than the control bilayers, as previously published work has shown (Mohamed et al., 2021). Overall, the capacitance measured is lower than published findings and this may also be attributed to the presence of PAH which is mediating the negative charge of PEDOT:PSS and serving as an additional interface between the bilayers and PEDOT: PSS. We note here that the resistance and capacitance values reported were obtained from a representative experiment.

3.3. OM supported bilayers contain native components from E. coli outer membranes

An advantage of using OMVs to form supported OM bilayers is the ability to incorporate into this platform native OM components that may

be targets of antibiotic activity, such as LPS and outer membrane proteins (OMPs). To verify the retention of native components in our OM bilayers, antibody binding was used to confirm the presence of LPS and OM protein components. OM bilayers were incubated with primary antibodies targeting lipid A of LPS or OMPs, and then labeled using fluorescent secondary antibodies before being imaged by TIRFM (Mohamed et al., 2021). Imaging of the OM bilayers showed significantly higher fluorescent signals for OM bilayer compared to the negative control, POPG-PEG5K bilayer, indicating the presence of native outer membrane materials. OM bilayers incubated with the Lipid A antibody displayed widespread bright fluorescence throughout the OM bilayer compared to the negative control (Fig. 3A). Lipid A is the lipid component of LPS and serves as a good confirmation of LPS in the OM bilayer. The positive fluorescent signals also demonstrate the retention of native LPS orientation, as the epitope for antibody binding is only available when LPS is facing away from the proximal surface.

Outer membrane proteins, however, are not as prevalent in the OM as LPS. As such, the detected antibody signal consisted of fewer, bright punctate spots (Fig. 3C). Counting these particles as individual protein components generated significantly higher fluorescence values measured in OM bilayers compared to the control bilayer, suggesting the presence of OMPs in our model OMs (Fig. 3D). This result also indicates that a fraction of the OMPs have maintained their native orientation in the SLB and are accessible to the antibody. Taken together, the results from the antibody binding experiments demonstrate the retention of native outer membrane components in the OM bilayer on PAH/PEDOT: PSS.

3.4. Polymyxin B, bacitracin, and meropenem interactions with OM bilayers are detected using EIS

To demonstrate the feasibility of using this outer membrane platform to monitor antibiotic-membrane interactions, we characterized the

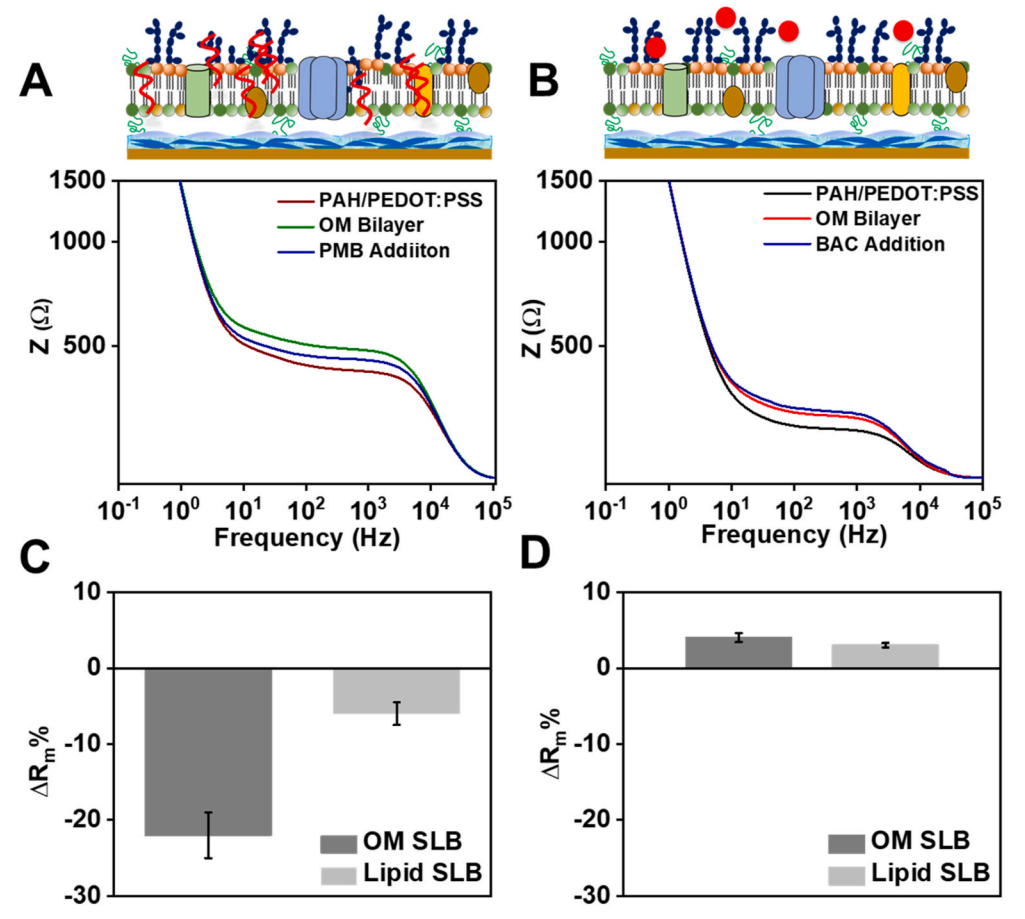


Fig. 4. EIS monitoring of PMB or BAC interaction with bacterial OM bilayer using PAH/PEDOT:PSS electrodes. Schematics of the biomembrane-integrated electrodes with the OM bilayer. Bode plots showing EIS response in the presence of 30 μ g/mL (A) PMB or (B) BAC(C, D). The relative changes in resistance between the OM bilayer and lipid (POPG-PEG5K) bilayer in the presence of PMB or BAC. Nyquist and phase plots with the addition of PMB or BAC can be found in the Supporting Information (Fig. S6).

interactions between the OM bilayer and three different antimicrobial compounds: polymyxin B (PMB), bacitracin (BAC), and meropenem (MER). We chose these three antimicrobial compounds, as their specific interactions with the OM depend on the composition of bacterial membranes and their well-characterized mechanisms of action can be used to validate the model membrane platform. PMB, a cationic antibiotic with hydrophobic peptide moieties, interacts strongly with the outer membrane of Gram-negative bacteria, in particular, the LPS layer (TrimbleMichael et al., 2016; Zavascki et al., 2007). In Gram-negative bacteria, PMB displaces divalent cations that mediate electrostatic repulsion between LPS molecules and results in destabilization and permeabilization of the OM as it inserts into the membrane (Brogden, 2005; Domingues et al., 2012). In contrast, the bulky nature of BAC molecules hinders their penetration through the OM of Gram-negative bacteria. This antibiotic is primarily used to treat Gram-positive bacteria, making it a good negative control for our platform validation. BAC's method of action hinders peptidoglycan layer synthesis by interfering with the dephosphorylation of C55-isoprenyl pyrophosphate (Stone and Strominger, 1971; Manat et al., 2014). Since the BAC binding site is not present in the OM, we expected no specific interaction with our model platform. Lastly, MER is a beta-lactam antibiotic known for permeating through proteins in the OM to covalently bind to penicillin-binding proteins and disrupt cell wall synthesis (Zhanel et al., 2010; Cornaglia et al., 1992). The small size and hydrophilic nature of MER allows for the passive diffusion of the antibiotic through the OM via outer membrane proteins such as porins. As such, we did not anticipate any changes in membrane resistance with MER treatment; we did, however, anticipate changes in capacitance.

To test whether our OM SLB platform could distinguish between these different antibiotic-membrane interactions, we utilized EIS to interrogate membrane properties in the presence of PMB, BAC, or MER. Impedance spectra of the PAH/PEDOT:PSS electrodes, after formation of OM bilayer and after addition of antibiotics to the bilayer, were recorded in succession. With addition of PMB, we observed a shift to lower impedance compared to the impedance of the OM bilayer alone (Fig. 4A). This observation is consistent with the expected mechanism of action of PMB, which involves increased membrane permeability due to disruption of LPS layer and reduced the insulating ability of the bilayer. In contrast, with addition of BAC, we found that the impedance response remains nearly the same before and after antibiotic addition (Fig. 4B), suggesting no changes occurred in the permeability of the OM bilayer. Both PMB and BAC membrane activity correspond to the expected behavior based on the known action of these drugs and substantiate the platform's ability to capture antibiotic activity against the OM.

To process the data, we extracted the change in membrane resistances using the equivalent circuit model and then normalized the changes with respect to the resistance values of the OM bilayer prior to the addition of the antibiotic. Theses relative changes in resistances $(\Delta R_m\%)$ of the OM bilayer in the presence of PMB or BAC are shown in Fig. 4C. Notably, a significant decrease in OM bilayer resistance ($-22 \pm$ 3%) is observed after the addition of PMB, whereas with the addition of BAC, the resistance remains nearly unchanged (4 \pm 0.3%). As PMB interacts strongly with LPS present in the bacterial membrane and permeabilizes the outer membrane, a decrease in membrane resistance is expected and confirmed. As our OM bilayer does not contain the components BAC binds with, we do not detect any significant changes in bilayer resistance. For our control case of POPG-PEG5K, we see little to no interaction of PMB and BAC with the POPG-PEG5K bilayer (Fig. S7). Some interaction of POPG lipids and PMB is expected due to electrostatic attraction between the cationic polypeptide and anionic lipids. However, as PMB has higher binding affinity to LPS, which is present specifically in the outer membrane, the extent of interaction of PMB is much

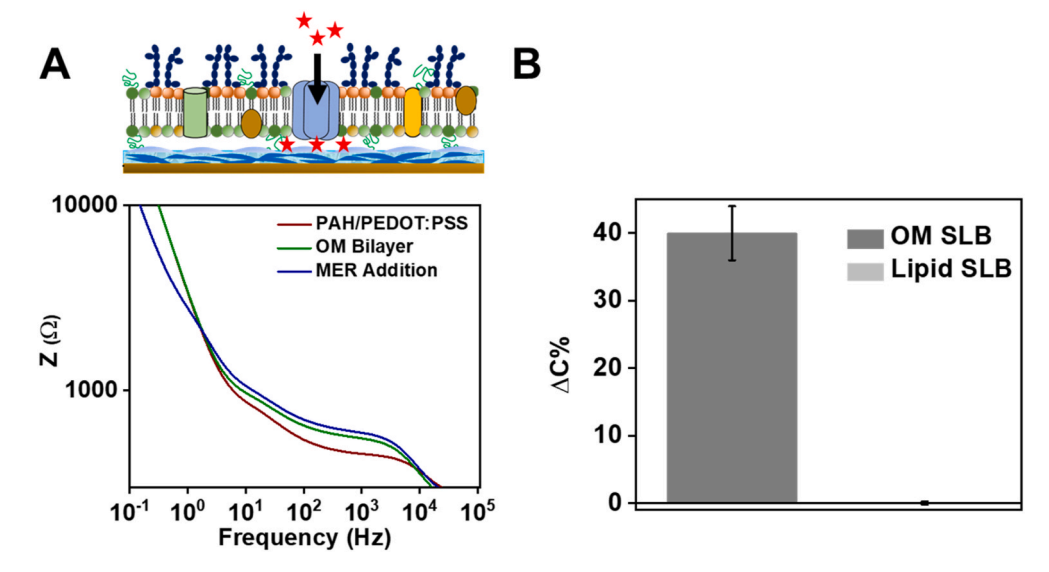


Fig. 5. EIS monitoring of changes in the bacterial bilayer with the addition of MER on PAH/PEDOT:PSS electrodes. A) Bode plots showing EIS response in the presence of $100 \,\mu\text{g/mL}$ MER. At low frequency, the difference in impedance before and after MER addition can be observed. B) The relative changes in capacitance calculated from the constant phase element between the OM bilayer and lipid (POPG-PEG5K) bilayer in the presence of MER.

higher in the OM bilayer ($-22\pm3\%$) compared to POPG-PEG5K bilayer ($-6\pm1.5\%$). On the other hand, BAC treatment results in a slight increase in resistance for both the OM bilayer (4 \pm 0.3%) and the POPG-PEG5K bilayer (3 \pm 0.6%), indicating a low level of non-specific membrane interaction in both cases. The impact of PMB and BAC on membrane capacitance is provided in the Supporting Information (Fig. S8).

Unlike PMB and BAC, the measured activity of MER was captured outside of the membrane resistance and capacitance changes. As MER diffuses through porins in the OM, a change in the constant phase element (Qp) describing the PAH/PEDOT:PSS layer was observed (Fig. 5A). This is seen in the Bode plot as the impedance shifts lower at low frequencies after addition of MER. After incubating the bilayers with MER and rinsing away excess MER, any antibiotic that diffused through the porins would remain under the bilayer at the interface between the OM and PAH/PEDOT:PSS, and thus, these changes would be measured at the PAH/PEDOT:PSS interface. Calculating the capacitance of the PAH/PEDOT:PSS, the change in capacitance (Δ C%) after incubation with MER is increased by 40 \pm 4% with the OM bilayer compared to $-0.02 \pm 0.2\%$ with the POPG-PEG5K bilayer that is devoid of OM proteins (Fig. 5B). Direct incubation of the antibiotic on PAH/PEDOT: PSS (no bilayers) does not result in a change in capacitance, signifying the presence of the OM bilayer is necessary for the responses observed (Figs. S9 and S10).

Collectively, these observations of the three distinct antibiotics demonstrate our OM platform's ability to identify the activity of membrane targeting antibiotics and to assess OM permeability of antibiotics via porins. Our results also establish the importance of capturing the full compositional complexity of the OM to accurately recapitulate the interactions of a variety of drugs having different mechanisms of action with the membrane. While these trends are reproducible and they recapitulate the actions of antibiotics, one limitation of this system stems from the variability that may occur from physical coating of PEDOT:PSS on the electrode surface. As a result, comparison of absolute values of resistance and capacitance across devices can be difficult. However, within the same electrode, there is a clear distinction when the antibiotic $\,$ interacts with the membrane and alters the membrane resistance, as we observe with PMB. Therefore, we report here the normalized results and standard deviations, which are a promising way to quantify these interactions.

4. Conclusion

Reconstituting a native-like bacterial OM on an electrically-conducting polymer surface opens new avenues for label-free, biosensing applications to identify novel antibiotics. In this article, we demonstrated a platform that is capable of screening antibiotic interactions in a bacterial OM model by measuring the change in electrical properties during bilayer formation and the membranes' interactions with disrupting compounds. This platform could be further expanded to create microelectrode arrays of different bacterial isolates for drug screening applications. Beyond that, OM bilayer arrays may also prove useful as bacterial phage screening tools and for better understanding the permeation of small molecules through the membrane. With more sophisticated device architectures that have higher time resolutions and sensitivities, such as bioelectronic transistors, detailed mechanistic studies of high-throughput drug interactions may also become possible.

CRediT authorship contribution statement

Surajit Ghosh: Investigation, Formal analysis, Data curation, Validation, Writing. Zeinab Mohamed: Investigation, Formal analysis, Data curation, Validation, Writing. Jung-Ho Shin: Methodology. Samavi Farnush Bint E Naser: Data curation. Karan Bali: Methodology. Tobias Dörr: Methodology, Resources. Róisín M. Owens: Supervision. Alberto Salleo: Supervision. Susan Daniel: Supervision.

Declaration of competing interest

The authors declare that they have no known competing financial interests or personal relationships that could have appeared to influence the work reported in this paper.

Acknowledgements:

This work was supported by the National Institutes of Health through Venatorx Pharmaceuticals (Grant Number R01AI136805). The authors acknowledge funding for this project, sponsored by the Defense Advanced Research Projects Agency (DARPA) Army Research Office and accomplished under Cooperative Agreement Number W911NF-18-2-0152. Z.M is supported by the National Science Foundation (Grant number DGE-1650441). This work made use of the Cornell Center for

Materials Research Shared Facilities, supported through the NSF MRSEC program (Grant number DMR-1719875). This work was performed in part at the Cornell NanoScale Facility, a member of the National Nanotechnology Coordinated Infrastructure (NNCI), which is supported by the National Science Foundation (Grant number NNCI-2025233). The views and conclusions contained in this document are those of the authors and should not be interpreted as representing the official policies, either expressed or implied, of DARPA or the Army Research Office or the U.S. Government or the National Science Foundation. The U.S. Government is authorized to reproduce and distribute reprints for Government purposes notwithstanding any copyright notation herein.

Appendix A. Supplementary data

Supplementary data to this article can be found online at https://doi.org/10.1016/j.bios.2022.114045.

References

- Brogden, K.A., 2005. Nat. Rev. Microbiol. 3, 238–250. Castellana, E.T., Cremer, P.S., 2006. Surf. Sci. Rep. 61, 429–444.
- Cho, N., Frank, C.W., Kasemo, B., Höök, F., 2010. Nat. Protoc. 5, 1096–1106. Cornaglia, G., Guan, L., Fontana, R., Satta, G., 1992. Antimicrob. Agents Chemother. 36, 1902–1908
- Delcour, A.H., 2009. Biochim. Biophys. Acta Protein Proteonomics 1794, 808–816. Diamanti, E., Gregurec, D., Rodríguez-Presa, M.J., Gervasi, C.A., Azzaroni, O., Moya, S. E., 2016. Langmuir 32, 6263–6271.
- Domingues, M.M., Inácio, R.G., Raimundo, J.M., Martins, M., Castanho, M.A.R.B., Santos, N.C., 2012. Biopolymers 98, 338–344.
- Epand, R.M., Walker, C., Epand, R.F., Magarvey, N.A., 2016. Biochim. Biophys. Acta Biomembr. 1858, 980–987.
- Gritsch, S., Nollert, P., Ja, F., Sackmann, E., 1998. Langmuir 7463, 3118–3125. Heath, G.R., Li, M., Polignano, I.L., Richens, J.L., Catucci, G., O'Shea, P., Sadeghi, S.J.,
- Gilardi, G., Butt, J.N., Jeuken, L.J.C., 2016. Biomacromolecules 17, 324–335. Hiroshi Nikaido, M.V., 1985. Microbiol. Rev. 49, 1–32.
- Hollmann, A., Martinez, M., Maturana, P., Semorile, L.C., Maffia, P.C., 2018. Front. Chem. 6, 1–13.
- Hsia, C.Y., Chen, L., Singh, R.R., DeLisa, M.P., Daniel, S., 2016. Sci. Rep. 6, 1–14. Hurdle, J.G., Neill, A.J.O., Chopra, I., Lee, R.E., 2011. Nat. Publ. Gr. 9, 62–75.
- Ishan Ghai, S.G., 2018. Infect. Drug Resist. 523–530. Jan, A.T., 2017. Front. Microbiol. 8, 1–11.
- Lin, J., Szymanski, J., Searson, P.C., Hristova, K., 2010. Langmuir 26, 12054–12059.

- Lin, J., Motylinski, J., Krauson, A.J., Wimley, W.C., Searson, P.C., Hristova, K., 2012. Langmuir 28, 6088–6096.
- Liu, H., Chen, W., Ober, C.K., Daniel, S., 2017. Langmuir 34, 1061-1072.
- Liu, H.-Y., Pappa, A.-M., Pavia, A., Pitsalidis, C., Thiburce, Q., Salleo, A., Owens, R.M., Daniel, S., 2020. Langmuir. https://doi.org/10.1021/acs.langmuir.0c00804.
- Manat, G., Roure, S., Auger, R., Bouhss, A., Barreteau, H., Mengin-Lecreulx, D., Touze, T., 2014. Microb. Drug Resist. 20, 199–214.
- McBroom, A.J., Johnson, A.P., Vemulapalli, S., Kuehn, M.J., 2006. J. Bacteriol. 188, 5385–5392.
- Mohamed, Z., Shin, J.H., Ghosh, S., Sharma, A.K., Pinnock, F., Farnush, S. Bint E Naser, Dörr, T., Daniel, S., 2021. ACS Infect. Dis. 7, 2707–2722.
- T. Nagakubo, N. Nomura and M. Toyofuku, Front. Microbiol., , DOI:10.3389/ fmicb.2019.03026.
- Orosz, K.S., Jones, I.W., Keogh, J.P., Smith, C.M., Griffin, K.R., Xu, J., Comi, T.J., Hall, H. K., Saavedra, S.S., 2016. Langmuir 32, 1577–1584.
- A.-M. Pappa, H.-Y. Liu, W. Traberg-Christensen, Q. Thiburce, A. Savva, A. Pavia, A. Salleo, S. Daniel and R.M. Owens, ACS Nano, , DOI:10.1021/acsnano.0c01330.
- Pappa, A.M., Inal, S., Roy, K., Zhang, Y., Pitsalidis, C., Hama, A., Pas, J., Malliaras, G.G., Owens, R.M., 2017. ACS Appl. Mater. Interfaces 9, 10427–10434.
- Puiggali-Jou, A., Pawlowski, J., Valle, L.J., Michaux, C., Perpe, E.A., 2018. ACS Omega 3, 9003–9019.
- Reimhult, E., Zäch, M., Höök, F., Kasemo, B., 2006. Langmuir 22, 3313-3319.
- Schneider, C.A., Rasband, W.S., Eliceiri, K.W., 2012. Nat. Methods 9, 671-675.
- Schwechheimer, C., Kuehn, 2017. Nat. Rev. Microbiol. 13, 605–619.
- Silhavy, T.J., Kahne, D., Walker, S., 2010. Cold Spring Harbor Perspect. Biol. 2, 1–16. Soumpasis, D.M., 1983. Biophys. J. 41, 95–97.
- Stone, K.J., Strominger, J.L., 1971. Proc. Natl. Acad. Sci. U.S.A. 68, 3223–3227.
- Su, H., Liu, H.Y., Pappa, A.M., Hidalgo, T.C., Cavassin, P., Inal, S., Owens, R.M., Daniel, S., 2019. ACS Appl. Mater. Interfaces 11, 43799–43810.
- Terrettaz, S., Mayer, M., Vogel, H., 2003. Langmuir 19, 5567-5569.
- M. Toyofuku, N. Nomura and L. Eberl, Nat. Rev. Microbiol., , DOI:10.1038/s41579-018-0112-2.
- Trimble, J., Michael, Mlynárčík, P., Kolář, M., Hancock, R.E.W., 2016. Cold Spring Harb. Perspect. Med 6, 1–22.
- Uribe, J., Liu, H.Y., Mohamed, Z., Chiou, A.E., Fischbach, C., Daniel, S., 2020. ACS Biomater. Sci. Eng. 6, 3945–3956.
- Ye, Q., Konradi, R., Textor, M., Reimhult, E., 2009. Langmuir 25, 13534–13539.
- Zavascki, A.P., Goldani, L.Z., Li, J., Nation, R.L., 2007. J. Antimicrob. Chemother. 60, 1206–1215.
- Zhanel, G.G., Wiebe, R., Dilay, L., Thomson, K., Rubinstein, E., 2010. Chemother. J. 19, 131–149.
- Zhang, L., Longo, M.L., Stroeve, P., 2000. Langmuir 5093-5099.
- Zhang, L., Vidu, R., Waring, A.J., Lehrer, R.I., Longo, M.L., Stroeve, P., 2002. Langmuir 1318–1331.
- Zhang, Y., Inal, S., Hsia, C.Y., Ferro, M., Ferro, M., Daniel, S., Owens, R.M., 2016. Adv. Funct. Mater. 26, 7304–7313.